ENTANGLEMENT ENTROPY IN VACUUM PAIR CREATION BY STRONG FIELDS

Deepak Sah[†], Manoranjan P. Singh

Theory and Simulations Lab, Theoretical and Computational Physics Section
Raja Ramanna Centre for Advanced Technology
Indore-452013, India
and
Homi Bhabha National Institute, Training School Complex
Anushakti Nagar, Mumbai 400094, India

Received 10 August 2025, accepted 28 November 2025, published online 8 December 2025

We investigate electron–positron pair production in single- and double-pulse Sauter-type electric fields, focusing on how temporal separation and field symmetry govern both momentum spectra and entanglement entropy. Using the quantum kinetic approach, we identify a universal three-stage evolution of the entanglement entropy: quasiparticle excitation, a transient oscillatory regime, and residual stabilization. Overlapping pulses produce broadened, irregular spectra with reduced final entropy, whereas well-separated pulses generate regular, high-contrast fringes and enhanced entanglement. This effect is particularly pronounced for antisymmetric configurations. We establish, for the first time, a quantitative link between momentum spectra and entropy: sharper, periodic spectral interference corresponds to stronger correlations between particle–antiparticle modes.

DOI:10.5506/APhysPolB.56.12-A6

1. Introduction

The creation of particle–antiparticle pairs from the quantum vacuum in strong electric fields, commonly known as the Schwinger effect, is one of the most striking non-perturbative predictions of quantum electrodynamics (QED) [1–3]. Originally formulated in the seminal work by Julian Schwinger in 1951, the theoretical framework provided an exact calculation of the vacuum decay rate in a constant electric field [4]. This phenomenon revealed the inherent instability of the vacuum under extreme conditions and opened new avenues for exploring quantum field theory (QFT) in background fields beyond perturbation theory. While the original formulation

[†] Corresponding author: dsah129@gmail.com

addressed constant fields, subsequent investigations have extended the analysis to time-dependent and spatially inhomogeneous configurations, revealing a rich structure of non-equilibrium dynamics [5–11].

Over the past two decades, advances in high-intensity laser technology [12, 13] have revived interest in the Schwinger mechanism. This is particularly true for scenarios where dynamically assisted or multipulse electric field configurations can reduce the exponential suppression of pair production rates [14–18]. In parallel, the study of quantum entanglement in relativistic QFT has gained considerable traction due to its fundamental importance and its practical applications in areas such as quantum information processing, condensed matter systems, and black hole physics [19–24]. A particularly important quantity in this context is the *entanglement entropy* — a measure of quantum correlations between subsystems — which has emerged as a key diagnostic for understanding quantum coherence, decoherence, and thermalization in field-theoretic settings [19, 21, 23, 25–27].

Entanglement entropy in the context of particle creation lies at the intersection of quantum information theory and non-equilibrium quantum field dynamics. In vacuum pair production, the external field interacts with the vacuum state to create particle–antiparticle pairs. It is well-established that particle–antiparticle pairs are always produced in an entangled state. The external electric field acts on the vacuum to generate these entangled pairs. Measures of quantum entanglement effectively characterize quantum correlations in quantum states and are independent of any specific observable.

For the Schwinger effect in Dirac or Klein–Gordon fields, the entanglement entropy between a subsystem and the rest — specifically, the entropy between particles in a produced pair, derived from the reduced density matrix — has been calculated [28–30]. Over the past decade, entanglement has been investigated for various field configurations, including uniform and time-dependent electric fields [31–35]. These studies have linked the entanglement to the number of produced particles or antiparticles and the degree of classicality in the resulting quantum state. For instance, Ebadi and Mirza [36] established that both constant and pulsed electric fields generate measurable entanglement between scalar and fermionic modes, demonstrating the dependence of the entropy per mode on field strength, momentum, and mass. However, such analyses were largely restricted to asymptotic (late-time) entanglement, leaving the integrated behavior over momentum modes and full time-dependent evolution unexplored. Furthermore, although the fundamental relationship between pair production and entanglement is established, the precise connection between field configuration parameters and the resulting entanglement patterns remains not completely explored. For example, a recent study on the entanglement entropy between left- and right-movers (equivalently between the positive- and negative-

frequency modes) examined its time evolution for a specific electric pulse profile [34]. That work also showed the equivalence between the statistical Gibbs entropy of the pairs and the entanglement entropy between the right-moving particles and left-moving antiparticles. A systematic investigation of how pulse shape and field symmetry collectively govern entanglement generation has not been fully addressed. Beyond single-pulse configurations, multi-pulse field trains have attracted significant attention as a promising setup for experimental pair creation [37, 38]. This feature makes multi-pulse configurations particularly interesting for studying entanglement generation and for understanding how the well-known oscillatory momentum spectrum in multi-pulse setups relates to quantum entanglement measures.

Motivated by these developments, we present a comprehensive investigation of the real-time evolution of entanglement entropy during electron–positron pair production driven by sequences of electric field pulses. The novel aspects of this work are:

(i) A systematic comparison of symmetric *versus* antisymmetric double-pulse configurations in both overlapping and well-separated regimes, revealing how field symmetry controls entanglement generation — a comparison not previously reported in the literature.

(ii) Establishment of a direct, quantitative link between the sharpness of interference fringes in the momentum spectrum and the final saturation value of entanglement entropy. This provides a new experimental signature that connects measurable momentum spectra with quantum information measures.

(iii) Identification of a universal three-stage evolution of entanglement entropy (quasiparticle excitation, transient oscillation, residual stabilization) across different field configurations, extending beyond previous studies that focused primarily on asymptotic entanglement.

Our primary focus is to determine how pulse symmetry and temporal separation affect both the momentum distribution function and the generation of quantum correlations. To study the momentum distribution function, we employ the Quantum Kinetic Equation (QKE), derived from the Dirac equation via a canonical Bogoliubov transformation [39]. This transformation is used to derive the single-particle distribution function from a set of three first-order coupled differential equations that are equivalent to the QKE. This approach yields a direct relation between the entanglement entropy and the distribution function.

We study the time evolution of the distribution function and entropy in time-dependent single- and double-pulse fields. This allows us to track the entropy through the three characteristic stages of vacuum pair creation:

(1) the quasiparticle stage driven by the external field,

(2) the transient regime dominated by quantum oscillations, and

(3) the asymptotic freeze-in phase where the momentum spectrum stabilizes and entropy saturates.

By resolving entropy for individual momentum modes, we can quantitatively connect spectral interference patterns to entanglement generation. Our results reveal that while the entropy dynamics follow the overall trend of the particle distribution function, the relationship is nonlinear in the transient regime, where interference effects are most significant. Symmetric pulse sequences tend to produce broader momentum spectra and higher final entropies, reflecting stronger entanglement across momentum sectors. In contrast, overlapping pulses suppress spectral coherence and reduce entropy generation, while well-separated pulses yield highly regular interference fringes correlated with enhanced final entanglement.

This paper is organized as follows: In Section 2, we introduce the theoretical formalism based on the Refs. [9, 40]. In Section 3, we analyze the results. In the last section we provide a brief conclusion.

Throughout the paper, we use natural units and set $\hbar = c = m = |e| = 1$, $e < 0$, and express all variables in terms of the electron mass unit.

2. Theoretical framework

The kinetic equation employed here has been derived by various methods [8, 39–42]. Here, we follow the formalism of [9], retaining only the elements essential for our analysis. The basic formulation of pair production can be derived from the Dirac equation for a fermionic field $\Psi(x)$ in an external electromagnetic field

$$(i\gamma^\mu \partial_\mu - e\gamma^\mu A_\mu - m)\,\Psi(x) = 0\,. \tag{1}$$

We consider a spatially homogeneous, time-dependent electric field along the z-axis, described by the vector potential in temporal gauge

$$A^\mu = (0, 0, 0, A(t))\,, \tag{2}$$

which generates the electric field

$$E(t) = -\frac{\mathrm{d}A(t)}{\mathrm{d}t}\,. \tag{3}$$

We seek solutions to the Dirac equation in the form of momentum eigenstates [39]

$$\psi^{(\pm)}_{\boldsymbol{k},r}(x) = \left[i\gamma^0\partial_0 + \gamma^j k_j - e\gamma^3 A(t) + m\right] \chi^{(\pm)}(\boldsymbol{k},t) R_r \, \mathrm{e}^{i\boldsymbol{k}\cdot\boldsymbol{x}} \,, \tag{4}$$

where $j = 1,2,3$, and the superscript $(\pm)$ denotes positive- and negative-frequency solutions, and R_r $(r = 1,2)$ are eigenvectors of the matrix $\gamma^0\gamma^3$

$$R_1 = \begin{pmatrix} 0 \\ 1 \\ 0 \\ -1 \end{pmatrix} \,, \qquad R_2 = \begin{pmatrix} 1 \\ 0 \\ -1 \\ 0 \end{pmatrix} \,, \tag{5}$$

satisfying $R_r^\dagger R_s = 2\delta_{rs}$.

The functions $\chi^{(\pm)}(\boldsymbol{k},t)$ satisfy an oscillator-type equation [7]

$$\ddot{\chi}^{(\pm)}(\boldsymbol{k},t) = -\left[\omega^2(\boldsymbol{k},t) + ie\dot{A}(t)\right] \chi^{(\pm)}(\boldsymbol{k},t) \,, \tag{6}$$

where the instantaneous energy is

$$\omega^2(\boldsymbol{k},t) = \varepsilon_\perp^2 + P^2(t) \,, \qquad \varepsilon_\perp^2 = m^2 + \boldsymbol{k}_\perp^2 \,, \qquad P(t) = k_z - eA(t) \,. \tag{7}$$

The field operators can be expanded in this basis as

$$\psi(x) = \sum_{r,\boldsymbol{k}} \left[\psi^{(-)}_{\boldsymbol{k}r}(x) b_{\boldsymbol{k}r}(t_0) + \psi^{(+)}_{\boldsymbol{k}r}(x) d^+_{-\boldsymbol{k}r}(t_0)\right] \,. \tag{8}$$

The operators $b_{\boldsymbol{k}r}(t_0)$, $b^\dagger_{\boldsymbol{k}r}(t_0)$ and $d_{\boldsymbol{k}r}(t_0)$, $d^\dagger_{\boldsymbol{k}r}(t_0)$ describe the annihilation and creation of electrons and positrons in the initial vacuum state $|0_{\mathrm{in}}\rangle$ at $t = t_0$. They satisfy the anticommutation relations

$$\left\{b_{\boldsymbol{k}r}(t_0), b^+_{\boldsymbol{k}'r'}(t_0)\right\} = \left\{d_{\boldsymbol{k}r}(t_0), d^+_{\boldsymbol{k}'r'}(t_0)\right\} = \delta_{rr'}\delta_{\boldsymbol{k}\boldsymbol{k}'} \,. \tag{9}$$

The time evolution in the external field mixes positive- and negative-energy states, leading to pair creation. This mixing is implemented through a time-dependent Bogoliubov transformation that diagonalizes the Hamiltonian at each instant

$$b_{\boldsymbol{k}r}(t) = \alpha_{\boldsymbol{k}}(t) b_{\boldsymbol{k}r}(t_0) + \beta_{\boldsymbol{k}}(t) d^+_{-\boldsymbol{k}r}(t_0) \,, \tag{10}$$

$$d_{\boldsymbol{k}r}(t) = \alpha_{-\boldsymbol{k}}(t) d_{\boldsymbol{k}r}(t_0) - \beta_{-\boldsymbol{k}}(t) b^+_{-\boldsymbol{k}r}(t_0) \,, \tag{11}$$

with the normalization condition

$$|\alpha_{\boldsymbol{k}}(t)|^2 + |\beta_{\boldsymbol{k}}(t)|^2 = 1 \,. \tag{12}$$

The field operator can be re-expanded in the instantaneous basis

$$\psi(x) = \sum_{r,\boldsymbol{k}} \left[\Psi^{(-)}_{\boldsymbol{k}r}(x) b_{\boldsymbol{k}r}(t) + \Psi^{(+)}_{\boldsymbol{k}r}(x) d^{+}_{-\boldsymbol{k}r}(t) \right], \tag{13}$$

where the new basis functions are related to the original ones by

$$\psi^{(-)}_{\boldsymbol{k}r}(x) = \alpha_{\boldsymbol{k}}(t)\Psi^{(-)}_{\boldsymbol{k}r}(x) - \beta^{*}_{\boldsymbol{k}}(t)\Psi^{(+)}_{\boldsymbol{k}r}(x), \tag{14}$$

$$\psi^{(+)}_{\boldsymbol{k}r}(x) = \alpha^{*}_{\boldsymbol{k}}(t)\Psi^{(+)}_{\boldsymbol{k}r}(x) + \beta_{\boldsymbol{k}}(t)\Psi^{(-)}_{\boldsymbol{k}r}(x). \tag{15}$$

The new basis functions have the form

$$\Psi^{(\pm)}_{\boldsymbol{k}r}(x) = \left[i\gamma^0\partial_0 + \gamma^j k_j - e\gamma^3 A(t) + m \right] \phi^{(\pm)}_{\boldsymbol{k}}(t) R_r \, \mathrm{e}^{\pm i\Theta(\boldsymbol{k},t)} \, \mathrm{e}^{i\boldsymbol{k}\cdot\boldsymbol{x}}, \tag{16}$$

with the dynamical phase

$$\Theta(\boldsymbol{k},t) = \int_{t_0}^{t} \mathrm{d}t' \omega\left(\boldsymbol{k},t'\right). \tag{17}$$

The time evolution of the system is governed by the dynamics of the Bogoliubov coefficients, which follow from the Dirac equation and the Bogoliubov transformation

$$\dot{\alpha}_{\boldsymbol{k}}(t) = \frac{eE(t)\varepsilon_{\perp}}{2\omega^2(\boldsymbol{k},t)} \beta^{*}_{\boldsymbol{k}}(t) \, \mathrm{e}^{2i\Theta(\boldsymbol{k},t)}, \tag{18}$$

$$\dot{\beta}^{*}_{\boldsymbol{k}}(t) = -\frac{eE(t)\varepsilon_{\perp}}{2\omega^2(\boldsymbol{k},t)} \alpha_{\boldsymbol{k}}(t) \, \mathrm{e}^{-2i\Theta(\boldsymbol{k},t)}. \tag{19}$$

These equations reveal a rapidly oscillating phase factor, $\mathrm{e}^{\pm 2i\Theta(\boldsymbol{k},t)}$, which complicates both numerical analysis and physical interpretation. To isolate the slower, physically relevant dynamics from these fast oscillations, we transition to the adiabatic particle number basis [43]. This is achieved by defining new creation and annihilation operators that absorb the dynamical phase

$$B_{\boldsymbol{k}r}(t) = b_{\boldsymbol{k}r}(t) \, \mathrm{e}^{-i\Theta(\boldsymbol{k},t)}, \tag{20}$$

$$D_{\boldsymbol{k}r}(t) = d_{\boldsymbol{k}r}(t) \, \mathrm{e}^{-i\Theta(\boldsymbol{k},t)}. \tag{21}$$

We obtain the equations of motion

$$\frac{\mathrm{d}B_{\boldsymbol{k}r}(t)}{\mathrm{d}t} = -\frac{eE(t)\varepsilon_{\perp}}{2\omega^2(\boldsymbol{k},t)} D^{+}_{-\boldsymbol{k}r}(t) + i[H(t), B_{\boldsymbol{k}r}(t)], \tag{22}$$

$$\frac{\mathrm{d}D_{\boldsymbol{k}r}(t)}{\mathrm{d}t} = \frac{eE(t)\varepsilon_{\perp}}{2\omega^2(\boldsymbol{k},t)} B^{+}_{-\boldsymbol{k}r}(t) + i[H(t), D_{\boldsymbol{k}r}(t)], \tag{23}$$

with the quasiparticle Hamiltonian

$$H(t) = \sum_{r,\boldsymbol{k}} \omega(\boldsymbol{k},t) \left(B^{+}_{\boldsymbol{k}r}(t) B_{\boldsymbol{k}r}(t) - D_{-\boldsymbol{k}r}(t) D^{+}_{-\boldsymbol{k}r}(t) \right) . \tag{24}$$

One can define the particle number, or distribution function, for electrons with momentum $\boldsymbol{k}$ and spin r as the expectation value of the number operator in the time-dependent basis, evaluated in the initial vacuum state

$$f_r(\boldsymbol{k},t) = \langle 0_{\rm in}| B^{\dagger}_{\boldsymbol{k}r}(t) B_{\boldsymbol{k}r}(t) |0_{\rm in}\rangle \, . \tag{25}$$

This expression can be evaluated directly using the Bogoliubov transformation that relates the time-evolved operators to the initial ones

$$f_r(\boldsymbol{k},t) = |\beta_{\boldsymbol{k}}(t)|^2 \, . \tag{26}$$

Similarly, the distribution function for positrons is defined as

$$\bar{f}_r(-\boldsymbol{k},t) = \langle 0_{\rm in}| D^{\dagger}_{-\boldsymbol{k}r}(t) D_{-\boldsymbol{k}r}(t) |0_{\rm in}\rangle \, , \tag{27}$$

which, upon evaluation, also yields $|\beta_{\boldsymbol{k}}(t)|^2$. This demonstrates the charge conjugation symmetry of the pair production process,

$$f_r(\boldsymbol{k},t) = \bar{f}_r(-\boldsymbol{k},t) \, , \tag{28}$$

confirming that electrons and positrons are produced in perfectly correlated pairs. Therefore, $|\beta_{\boldsymbol{k}}(t)|^2$ serves as the fundamental distribution function in the quasiparticle representation [43].

The time evolution of this distribution function is derived from the Heisenberg equations of motion, leading to

$$\frac{{\rm d}f_r(\boldsymbol{k},t)}{{\rm d}t} = -\frac{eE(t)\varepsilon_\perp}{\omega^2(\boldsymbol{k},t)} {\rm Re}\left\{ \mathcal{C}_r(\boldsymbol{k},t) \right\} \, , \tag{29}$$

where the particle–antiparticle correlation function

$$\mathcal{C}_r(\boldsymbol{k},t) = \langle 0_{\rm in}| D_{-\boldsymbol{k}r}(t) B_{\boldsymbol{k}r}(t) |0_{\rm in}\rangle \tag{30}$$

encodes the quantum coherence of the created pairs. This complex function evolves according to

$$\frac{{\rm d}\,\mathcal{C}_r(\boldsymbol{k},t)}{{\rm d}t} = \frac{eE(t)\varepsilon_\perp}{2\omega^2(\boldsymbol{k},t)} \left[2 f_r(\boldsymbol{k},t) - 1 \right] - 2i\omega(\boldsymbol{k},t) \mathcal{C}_r(\boldsymbol{k},t) \, . \tag{31}$$

To formulate a system amenable to both numerical solution and physical interpretation, we separate the correlation function into its real and imaginary parts

$$\mathcal{C}_r(\boldsymbol{k},t) = u_r(\boldsymbol{k},t) + iv_r(\boldsymbol{k},t)\,, \tag{32}$$

where $u_r(\boldsymbol{k},t) \equiv \mathrm{Re}[\mathcal{C}_r]$ represents vacuum polarization effects, and $v_r(\boldsymbol{k},t) \equiv \mathrm{Im}[\mathcal{C}_r]$ denotes some kind of countering term to the pair production.

Substituting this decomposition yields the final, closed set of quantum kinetic equations

$$\begin{aligned}
\frac{\mathrm{d}f(\boldsymbol{k},t)}{\mathrm{d}t} &= \frac{eE(t)\epsilon_\perp}{2\omega^2(\boldsymbol{k},t)}u(\boldsymbol{k},t)\,,\\
\frac{\mathrm{d}u(\boldsymbol{k},t)}{\mathrm{d}t} &= \frac{eE(t)\epsilon_\perp}{\omega^2(\boldsymbol{k},t)}\left[1-2f(\boldsymbol{k},t)\right] - 2\omega(\boldsymbol{k},t)v(\boldsymbol{k},t)\,,\\
\frac{\mathrm{d}v(\boldsymbol{k},t)}{\mathrm{d}t} &= 2\omega(\boldsymbol{k},t)u(\boldsymbol{k},t)\,,
\end{aligned} \tag{33}$$

where the spin index r is omitted due to spin independence. This system provides a complete dynamical description of vacuum pair production, where the Pauli exclusion principle is manifest in the $[1-2f(\boldsymbol{k},t)]$ factor, suppressing production as states become occupied. This set of coupled differential equations for $f(\boldsymbol{k},t)$, $u(\boldsymbol{k},t)$, and $v(\boldsymbol{k},t)$ possesses a first integral of motion given by

$$\left(1-2f(\boldsymbol{k},t)\right)^2 + u^2(\boldsymbol{k},t) + v^2(\boldsymbol{k},t) = 1\,. \tag{34}$$

It may be noted here that this system of equations can be equivalently expressed as a single non-Markovian integral equation [39]

$$\frac{\mathrm{d}f(\boldsymbol{k},t)}{\mathrm{d}t} = \frac{eE(t)\epsilon_\perp^2}{2\omega^2(\boldsymbol{k},t)}\int_{-\infty}^{t}\mathrm{d}t'\,\frac{eE\left(t'\right)}{\omega^2\left(\boldsymbol{k},t'\right)}\left[1-2f\left(\boldsymbol{k},t'\right)\right]\cos\left[2\Theta\left(\boldsymbol{k},t,t'\right)\right]\,, \tag{35}$$

where $\Theta(\boldsymbol{k},t,t') = \Theta(\boldsymbol{k},t) - \Theta(\boldsymbol{k},t')$. This form explicitly demonstrates the memory effects and quantum coherence inherent in the pair production process [44, 45].

The quantum kinetic equations (33) form the basis for our numerical investigation of entanglement entropy generation during vacuum pair production in time-dependent electric fields.

For the remainder of this work, we simplify the analysis by setting the transverse momentum to zero ($k_\perp = 0$) and denote the longitudinal momentum simply by k (*i.e.*, $k_z = k$).

2.1. Entanglement entropy

The primary measure of quantum correlations in this work is the entanglement entropy between the left-moving and right-moving particles, a natural bipartition induced by the directional electric field [34, 36]. For a pure initial vacuum state, the entanglement entropy, for a given momentum mode k is defined in terms of the Bogoliubov coefficients

$$S(k,t) = -\left[|\alpha_k(t)|^2 \log|\alpha_k(t)|^2 + |\beta_k(t)|^2 \log|\beta_k(t)|^2\right] . \tag{36}$$

Using the relation $f(k,t) = |\beta_k(t)|^2$, which defines the particle distribution function, and the normalization condition $|\alpha_k(t)|^2 + |\beta_k(t)|^2 = 1$, which implies $|\alpha_k(t)|^2 = 1 - f(k,t)$, the entanglement entropy can be expressed directly in terms of the distribution function obtained from the quantum kinetic equations. The resulting expression

$$S(k,t) = -\left[(1-f(k,t))\log(1-f(k,t)) + f(k,t)\log f(k,t)\right] \tag{37}$$

reveals itself as the Shannon entropy of a binary probability distribution. In this interpretation, $f(k,t)$ represents the probability that a specific momentum mode k is occupied by a particle, while $(1-f(k,t))$ is the probability that it remains unoccupied (*i.e.* in the vacuum state). This formulation makes the profound connection between particle dynamics and information theory explicit: the act of pair production from the vacuum directly injects quantum information into the system, and the distribution function $f(k,t)$ serves as the complete repository of this information. The total entanglement entropy is then obtained by integrating over all momentum modes

$$S(t) = \int \frac{\mathrm{d}k}{2\pi} S(k,t) . \tag{38}$$

This formulation reveals a profound connection: the distribution function $f(k,t)$, which governs particle production, also encodes complete information about the quantum entanglement generated by the external field. A key result, established in [34], is the equivalence between this entanglement entropy and the Gibbs entropy of the final-state particle distribution, bridging quantum information theory and thermodynamics.

The quantum kinetic equations (33) for $f(k,t), u(k,t), v(k,t)$, coupled with Eq. (35) for $S(t)$, form the complete set of equations that we solve numerically in the following section to investigate the dynamics of pair creation and entanglement generation.

2.2. Numerical implementation

The system of coupled differential equations (35) was solved numerically using a variable-step, variable-order Adams–Bashforth–Moulton PECE

solver (implementation `ode113` in MATLAB) [46], chosen for its high efficiency in handling the non-stiff, oscillatory nature of the equations. Initial conditions were set at a time $t_{\rm in} = -10\tau$, τ is the pulse duration of the time-dependent Sauter-pulsed field, sufficiently before the pulse activation to represent the vacuum state

$$f(k, t_{\rm in}) = 10^{-16}\,, \qquad u(k, t_{\rm in}) = v(k, t_{\rm in}) = \frac{10^{-16}}{\sqrt{2}}\,. \tag{39}$$

The conservation of the first integral, Eq. (34), was monitored throughout the evolution. Computations were performed with stringent relative and absolute error tolerances of 10^{-14} and 10^{-15}, respectively.

3. Results

In this section, we present the evolution of the single-particle distribution function, $f(k,t)$, and the entanglement entropy, $S(t)$, during vacuum pair production. All results are obtained by numerically solving the quantum kinetic equations (33) for the Sauter-type pulses with a field strength of $E_0 = 0.2E_{\rm c}$, using the methods detailed in Section 2. Throughout this section, all quantities are expressed in natural units based on the electron mass m; thus, time has units of m^{-1}, and the critical Schwinger field is $E_{\rm c} = m^2/|e|$.

Our analysis proceeds in two stages. First, we establish a baseline by identifying a universal three-stage dynamical evolution using a single-pulse field. Second, we systematically investigate how this evolution is controlled and enhanced using double-pulse sequences, focusing on the critical roles of temporal separation and field symmetry.

3.1. Single-pulse

To demonstrate a baseline, we first analyze pair production driven by a single-pulse electric field of the Sauter type. The electric field is given by

$$E(t) = E_0\,\mathrm{sech}^2\left(\frac{t}{\tau}\right)\,, \tag{40}$$

where E_0 denotes the field amplitude and τ characterizes the pulse duration.

Figure 1 shows the time evolution of the distribution function, $f(t)$ and entanglement entropy $S(t)$ for pulse durations $\tau = 5$ and $\tau = 10$ with fixed momentum $k = 0$. The virtual electron–positron pairs in the initial vacuum state interact with the electric field (40). Initially, the pairs are off-shell. As time progresses, they acquire energy from the field and approach an on-shell mass configuration [47]. During this process, the distribution function exhibits three distinct dynamical stages [43, 48, 49].

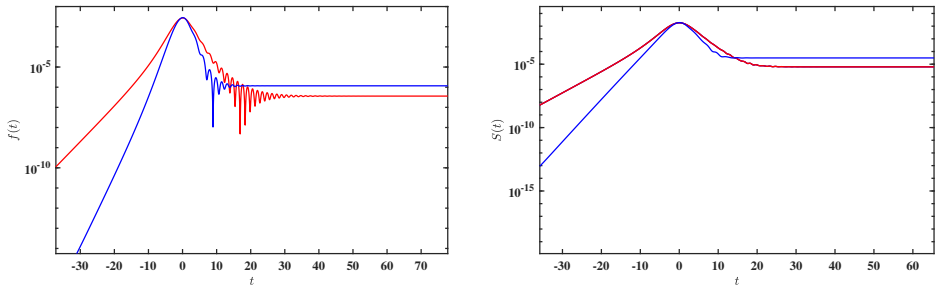

Fig. 1. Evolution of $f(t)$ (left) and entanglement entropy $S(t)$ (right) for Sauter pulse electric field with $\tau = 10$ (red), 5 (blue), and $E_0 = 0.2$, and all the units are taken in electron mass unit.

In both the long- and short-pulse cases, the system begins in the vacuum state at $t \to -\infty$ with $f(t) \approx 0$. As the electric field increases, the vacuum becomes unstable, exciting virtual pairs and causing $f(t)$ to rise rapidly. It peaks near $t = 0$, where the field strength is maximal. In Fig. 1, this behavior is clearly visible: for both pulse durations, the rise in $f(t)$ indicates that pair creation occurs predominantly during the central part of the pulse. After the peak, $f(t)$ declines rapidly, followed by a transient regime with strong oscillations. The extent and persistence of these oscillations depend strongly on the pulse duration. For the longer pulse ($\tau = 10$), the transient oscillations are more prominent and decay more slowly, reflecting stronger coherence and interference across the extended interaction time. In contrast, for $\tau = 5$, the transient stage is shorter-lived and $f(t)$ stabilizes more quickly. In both cases, $f(t)$ asymptotically approaches a constant value at late times ($t \gg \tau$), representing the final yield of real particles.

The time evolution of $f(t)$ can thus be interpreted in terms of three distinct dynamical stages:

1. Quasiparticle stage: At early times, the growing electric field excites virtual pairs from the vacuum. The increase in $f(t)$ is smooth and the system remains highly coherent.

2. Transient stage: Around the field peak, rapid oscillations appear in $f(t)$, reflecting the interplay between particle production, annihilation, and interference between modes with different production times.

3. Residual particle stage: Once the field has diminished, the system enters a stationary state with a fixed particle number.

The final value of $f(t)$ depends on the pulse duration, with longer pulses generating more particles. The pronounced difference in oscillatory behavior between the two pulses illustrates how longer field durations enhance quantum coherence and permit richer dynamics during the transient stage.

To characterize the quantum correlations, we compute the entanglement entropy using Eq. (38), performing the momentum integration numerically via trapezoidal method (MATLAB trapz function) [50]. The entanglement entropy $S(t)$, shown in the right panel of Fig. 1, starts from zero, consistent with the initial pure vacuum state. It increases steadily as the field drives particle production, reaching a maximum around the pulse peak — the point of maximal entanglement. Unlike $f(t)$, the entropy evolves smoothly through the transient regime, showing no pronounced oscillations. This indicated that $S(t)$ is an integrated measure of quantum correlations, less sensitive to fine-grained phase coherence than the distribution function. This smoothing is expected since entropy is a nonlinear function of $f(t)$ and inherently averages over microscopic quantum phases. At late times, $S(t)$ saturates to a residual value, which is higher for the longer pulse $\tau = 10$, consistent with the larger particle yield and confirming that longer field exposure generated greater entanglement. The simultaneous examination of $f(t)$ and $S(t)$ confirms, we observe a universal three-stage behavior.

In the quasiparticle stage, the electric field distorts the vacuum, causing a monotonic rise in both $f(t)$ and $S(t)$, with particles still largely virtual and strongly entangled. The transient stage occurs near $t = 0$, when $f(t)$ oscillates while $S(t)$ saturates near its maximum. Finally, in the residual particle stage, as the field vanishes, the system settles into a stationary mixed state with constant $f(t)$ and $S(t)$, effectively freezing the entanglement.

3.2. Double-pulse interference and entanglement

We now consider two sequential Sauter-type pulses to explore how field structure controls pair production and entanglement. The electric field is modeled as

$$E_{\pm}(t) = E_0 \left[\operatorname{sech}^2\left(\frac{t+T/2}{\tau}\right) \pm \operatorname{sech}^2\left(\frac{t-T/2}{\tau}\right) \right], \tag{41}$$

where E_0 is the peak field strength, τ is the pulse width, and T is the temporal separation. The plus and minus signs correspond to symmetric (S) and antisymmetric (A) configurations, respectively.

We examine both overlapping ($T = 17$) and well-separated ($T = 68$) regimes (in units of m^{-1}). Figure 2 shows $f(t)$ and $S(t)$ for the symmetric configuration. For overlapping pulses (green), the pulses merge into a single broadened profile. The distribution function $f(t)$ rises smoothly to

a peak, exhibiting only weak oscillations before saturation. In contrast, for well-separated pulses (magenta), $f(t)$ develops two distinct plateaus — one for each pulse. The second pulse acts on a pre-excited vacuum, inducing strong oscillations that signal temporal interference between the two creation events. The entropy $S(t)$ mirrors this trend smoothly. For overlapping pulses, $S(t)$ grows monotonically to a saturation value. For well-separated pulses, $S(t)$ exhibits a clear two-step growth, reaching a higher final value, which demonstrates that multi-pulse interference enhances entanglement generation.

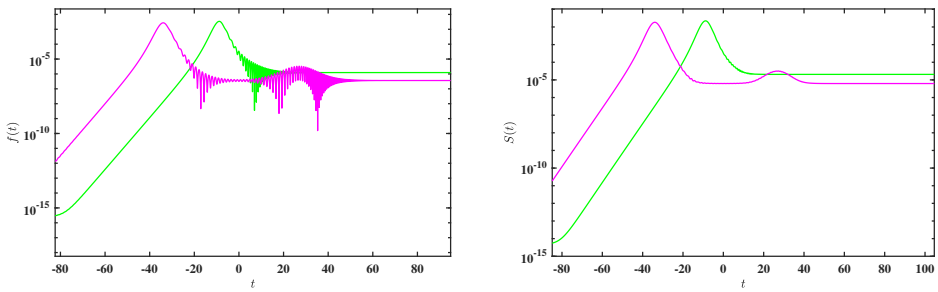

Fig. 2. Evolution of $f(t)$ (left) and entanglement entropy $S(t)$ (right) for particles for two pulses in the symmetric configuration with $T = 17$ (green) overlapping pulses and 68 (magenta) well-separated pulses.

Figure 3 shows the results for the antisymmetric configuration. For overlapping pulses, destructive interference between the oppositely signed fields suppresses the net vector potential, resulting in slow growth of $f(t)$ with minimal oscillations. For well-separated pulses, the first pulse increases $f(t)$, but the second pulse partially reverses the excitation, leading to non-monotonic behavior and oscillations. The final particle yield is lower than in the sym-

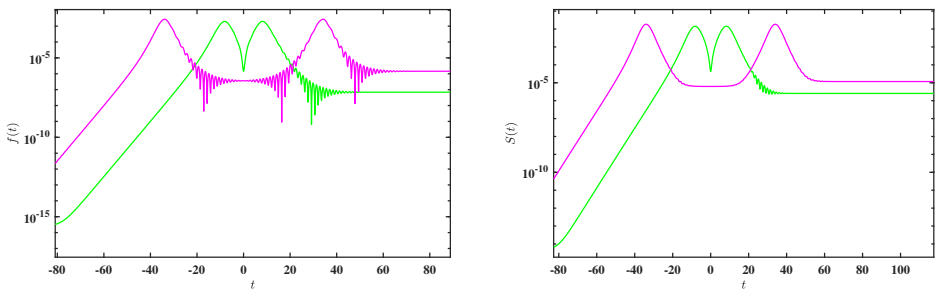

Fig. 3. Evolution of $f(t)$ (on the left) and entanglement entropy $S(t)$ (on the right) for particles for two pulses in the antisymmetric configuration with $T = 17$ (green) overlapping pulses and 68 (magenta) well-separated pulses.

metric case, underscoring how field symmetry controls vacuum excitation. The evolution of entropy is also suppressed. For overlapping pulses, $S(t)$ grows modestly to a low saturation value. For well-separated pulses, $S(t)$ shows two growth stages, but the second is weaker, suggesting the second pulse partially decoheres the state created by the first.

The connection between spectral interference and quantum correlations is revealed in the asymptotic momentum distributions (Figs. 4 and 5). For the symmetric configuration (Fig. 4), overlapping pulses produce a broad, featureless spectrum, while well-separated pulses yield two distinct, sharp peaks. For the antisymmetric configuration (Fig. 5), overlapping pulses generate irregular, asymmetric fringes, whereas well-separated pulses produce a high-contrast, periodic interference pattern — a clear signature of coherent pair creation at two distinct times. This coherent momentum-space structure is directly linked to the quantum correlations between the produced pairs.

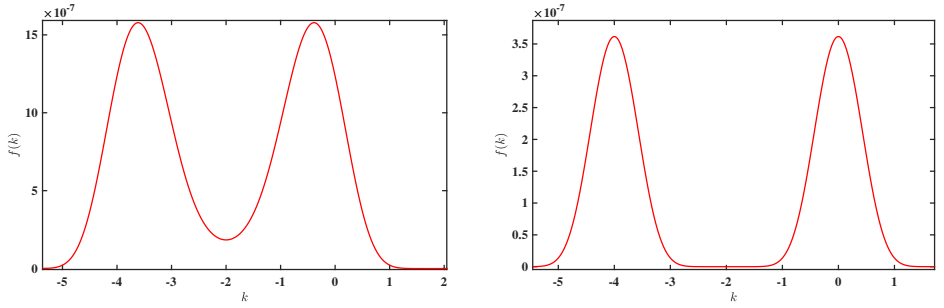

Fig. 4. Spectra of produced particles for two pulses in the symmetric configuration. Left: Overlapping pulses. Right: Well-separated pulses.

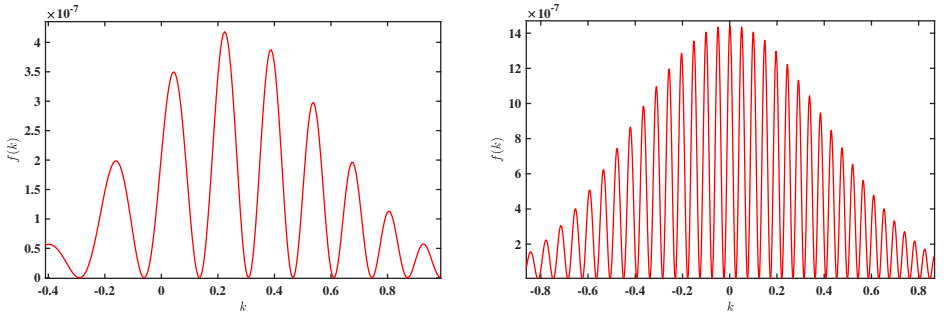

Fig. 5. Spectra of produced particles for two pulses in the antisymmetric configuration. Left: Overlapping pulses. Right: Well-separated pulses.

This link is quantified in Fig. 6, which compares the time-evolution of the total entanglement entropy $S(t)$ for symmetric (brown) and antisymmetric (blue) configurations. In the overlapping regime, the antisymmetric field produces a rapid entropy rise followed by a secondary peak, while the symmetric field leads to a smoother evolution and a lower final entropy. In the well-separated regime, both configurations exhibit a two-stage entropy growth, but the antisymmetric case achieves a higher final value, correlating with its sharper momentum-space interference fringes.

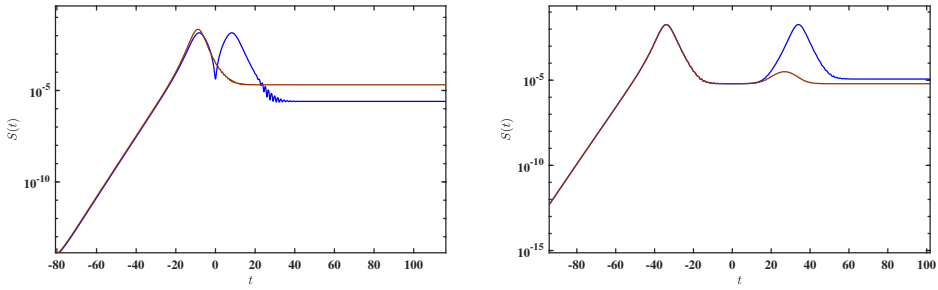

Fig. 6. Entanglement entropy as a function of time for antisymmetric (blue) and symmetric (brown) configurations of two pulses configuration. Left: Overlapping pulses $T = 17$. Right: Well-separate $T = 68$.

These results establish a clear correspondence: sharper, periodic momentum-space fringes are associated with stronger mode correlations and higher final entanglement entropy. Conversely, broader, irregular spectra correspond to weaker correlations and lower entropy. Thus, the entanglement entropy $S(t)$ serves as a sensitive, time-resolved probe of spectral coherence in strong-field QED, providing a unified framework that links observable interference phenomena to quantum information measures.

4. Summary

We have investigated the generation of electron–positron entanglement during vacuum pair creation driven by sequences of the Sauter-type electric field pulses. Within the quantum kinetic framework, we tracked the simultaneous evolution of the distribution function and the entanglement entropy $S(t)$, establishing a direct connection between spectral interference patterns and quantum correlations. Our study compared symmetric and antisymmetric pulse configurations across both overlapping and well-separated temporal regimes. In all cases, the entanglement entropy $S(t)$ exhibits a universal three-stage evolution:

1. A quasiparticle excitation stage, where the external field triggers pair creation and entropy growth.
2. A transient stage, characterized by oscillations in the distribution function that are mirrored by modulations in $S(t)$.
3. Residual particle stage, where both quantities saturate to final values that characterize the resulting entangled state.

The temporal separation T between pulses is a key control parameter. In the overlapping regime, the pulses merge into a single broad interaction, producing smooth momentum spectra with weak, irregular oscillations, reduced mode selectivity, and lower final entropy. In contrast, the well-separated regime produces spectra with strong coherence, featuring high-contrast, regularly spaced fringes whose spacing decreases with increasing T. For antisymmetric pulses, these fringes are especially sharp and symmetric, resembling a two-slit interference pattern in momentum space. This configuration also produces two distinct stages of entropy growth — one for each pulse. The antisymmetric, well-separated case yields the highest final entanglement, demonstrating that field symmetry is a powerful tool for enhancing or suppressing quantum correlations.

Our results establish a definitive link: sharper, periodic momentum spectra correspond to stronger mode correlations and higher final entanglement, whereas broader, irregular spectra indicate diluted correlations and reduced entropy. As momentum spectra are experimentally accessible in high-intensity laser facilities and analogue platforms, they serve as a practical and observable indicator of quantum entanglement in strong-field QED.

D. Sah acknowledges the financial assistance provided by the Raja Ramanna Center for Advanced Technology (RRCAT) and the Homi Bhabha National Institute (HBNI) for carrying out this research work.

REFERENCES

[1] P.A.M. Dirac, «The quantum theory of the electron», *Proc. R. Soc. Lond. A* **117**, 610 (1928).

[2] C.D. Anderson, «The Positive Electron», *Phys. Rev.* **43**, 491 (1933).

[3] F. Sauter, «Über das Verhalten eines Elektrons im homogenen elektrischen Feld nach der relativistischen Theorie Diracs», *Z. Phys.* **69**, 742 (1931).

[4] J.S. Schwinger, «On Gauge Invariance and Vacuum Polarization», *Phys. Rev.* **82**, 664 (1951).

[5] L.V. Keldysh, «Ionization in the Field of a Strong Electromagnetic Wave», *J. Exp. Theor. Phys.* **20**, 1307 (1965).

[6] E. Brezin, C. Itzykson, «Pair Production in Vacuum by an Alternating Field», *Phys. Rev. D* **2**, 1191 (1970).

[7] A.I. Nikishov, «Barrier scattering in field theory removal of Klein paradox», *Nucl. Phys. B* **21**, 346 (1970).

[8] F. Hebenstreit, R. Alkofer, H. Gies, «Schwinger pair production in space and time-dependent electric fields: Relating the Wigner formalism to quantum kinetic theory», *Phys. Rev. D* **82**, 105026 (2010), arXiv:1007.1099 [hep-ph].

[9] S.A. Smolyansky *et al.*, «Dynamical derivation of a quantum kinetic equation for particle production in the Schwinger mechanism», arXiv:hep-ph/9712377.

[10] D.B. Blaschke *et al.*, «Dynamical Schwinger effect and high-intensity lasers. Realising nonperturbative QED», *Eur. Phys. J. D* **55**, 341 (2009), arXiv:0811.3570 [physics.plasm-ph].

[11] N. Tanji, «Dynamical view of pair creation in uniform electric and magnetic fields», *Ann. Phys.* **324**, 1691 (2009) arXiv:0810.4429 [hep-ph].

[12] T. Heinzl, A. Ilderton, «Exploring high-intensity QED at ELI», *Eur. Phys. J. D* **55**, 359 (2009), arXiv:0811.1960 [hep-ph].

[13] A. Ringwald, «Pair production from vacuum at the focus of an X-ray free electron laser», *Phys. Lett. B* **510**, 107 (2001), arXiv:hep-ph/0103185.

[14] E. Akkermans, G.V. Dunne, «Ramsey Fringes and Time-Domain Multiple-Slit Interference from Vacuum», *Phys. Rev. Lett.* **108**, 030401 (2012), arXiv:1109.3489 [hep-th].

[15] G. Torgrimsson, C. Schneider, J. Oertel, R. Schützhold, «Dynamically assisted Sauter–Schwinger effect — non-perturbative *versus* perturbative aspects», *J. High Energy Phys.* **2017**, 043 (2017), arXiv:1703.09203 [hep-th].

[16] M. Orthaber, F. Hebenstreit, R. Alkofer, «Momentum spectra for dynamically assisted Schwinger pair production», *Phys. Lett. B* **698**, 80 (2011), arXiv:1102.2182 [hep-ph].

[17] R. Schutzhold, H. Gies, G. Dunne, «Dynamically Assisted Schwinger Mechanism», *Phys. Rev. Lett.* **101**, 130404 (2008), arXiv:0807.0754 [hep-th].

[18] Z.L. Li, B.S. Xie, Y.J. Li, «Boson pair production in arbitrarily polarized electric fields», *Phys. Rev. D* **100**, 076018 (2019), arXiv:1908.10556 [quant-ph].

[19] Y. Shi, «Entanglement in relativistic quantum field theory», *Phys. Rev. D* **70**, 105001 (2004), arXiv:hep-th/0408062.

[20] N. Laflorencie, «Quantum entanglement in condensed matter systems», *Phys. Rep.* **646**, 1 (2016), arXiv:1512.03388 [cond-mat.str-el].

[21] T. Fan, Q. Liu, J. Jing, J. Wang, «Quantum metrology of Schwinger effect», *Eur. Phys. J. C* **84**, 896 (2024).

[22] R. Horodecki, P. Horodecki, M. Horodecki, K. Horodecki, «Quantum entanglement», *Rev. Mod. Phys.* **81**, 865 (2009), arXiv:quant-ph/0702225.

[23] S. Mukohyama, M. Seriu, H. Kodama, «Can the entanglement entropy be the origin of black hole entropy?», *Phys. Rev. D* **55**, 7666 (1997), arXiv:gr-qc/9701059.

[24] T. Colas, J. Grain, G. Kaplanek, V. Vennin, «In-in formalism for the entropy of quantum fields in curved spacetimes», *J. Cosmol. Astropart. Phys.* **2024**, 047 (2024), arXiv:2406.17856 [hep-th].

[25] I. Fuentes, R.B. Mann, E. Martin-Martínez, S. Moradi, «Entanglement of Dirac fields in an expanding spacetime», *Phys. Rev. D* **82**, 045030 (2010), arXiv:1007.1569 [quant-ph].

[26] Y. Li, Q. Mao, Y. Shi, «Schwinger effect of a relativistic boson entangled with a qubit», *Phys. Rev. A* **99**, 032340 (2019), arXiv:1812.08534 [hep-th].

[27] S.Y. Lin, C.H. Chou, B.L. Hu, «Quantum entanglement and entropy in particle creation», *Phys. Rev. D* **81**, 084018 (2010), arXiv:1001.4922 [gr-qc].

[28] S.P. Gavrilov, D.M. Gitman, A.A. Shishmarev, «States of charged quantum fields and their statistical properties in the presence of critical potential steps», *Phys. Rev. A* **99**, 052116 (2019), arXiv:1901.01217 [hep-th].

[29] Y. Li, Y. Dai, Y. Shi, «Pairwise mode entanglement in Schwinger production of particle–antiparticle pairs in an electric field», *Phys. Rev. D* **95**, 036006 (2017), arXiv:1612.01716 [hep-th].

[30] S.P. Gavrilov, D.M. Gitman, A.A. Shishmarev, «Statistical properties of states in QED with unstable vacuum», *Phys. Rev. A* **91**, 052106 (2015), arXiv:1412.8506 [hep-th].

[31] S. Grieninger, D.E. Kharzeev, I. Zahed, «Entanglement entropy in a time-dependent holographic Schwinger pair creation», *Phys. Rev. D* **108**, 126014 (2023), arXiv:2310.12042 [hep-th].

[32] W. Kou, X. Chen, «Exploring quantum entanglement in chiral symmetry partial restoration with 1+1 string model», *Phys. Lett. B* **853**, 138675 (2024), arXiv:2401.16673 [hep-ph].

[33] A. Lewkowycz, J. Maldacena, «Exact results for the entanglement entropy and the energy radiated by a quark», *J. High Energy Phys.* **2014**, 025 (2014), arXiv:1312.5682 [hep-th].

[34] A. Florio, D.E. Kharzeev, «Gibbs entropy from entanglement in electric quenches», *Phys. Rev. D* **104**, 056021 (2021), arXiv:2106.00838 [hep-th].

[35] P.J. Ehlers, «Entanglement between valence and sea quarks in hadrons of 1+1 dimensional QCD», *Ann. Phys.* **452**, 169290 (2023), arXiv:2209.09867 [hep-ph].

[36] Z. Ebadi, B. Mirza, «Entanglement generation by electric field background», *Ann. Phys.* **351**, 363 (2014), arXiv:1410.3130 [quant-ph].

[37] Z.L. Li *et al.*, «Enhanced pair production in strong fields by multiple-slit interference effect with dynamically assisted Schwinger mechanism», *Phys. Rev. D* **89**, 093011 (2014).

[38] F. Fillion-Gourdeau, D. Gagnon, C. Lefebvre, S. MacLean, «Time-domain quantum interference in graphene», *Phys. Rev. B* **94**, 125423 (2016), arXiv:1607.02055 [cond-mat.mes-hall].

[39] S.M. Schmidt *et al.*, «A Quantum Kinetic Equation for Particle Production in the Schwinger Mechanism», *Int. J. Mod. Phys. E* **7**, 709 (1998), arXiv:hep-ph/9809227.

[40] J. Rau, B. Müller, «From reversible quantum microdynamics to irreversible quantum transport», *Phys. Rep.* **272**, 1 (1996), arXiv:nucl-th/9505009.

[41] J. Rau, «Pair production in the quantum Boltzmann equation», *Phys. Rev. D* **50**, 6911 (1994), arXiv:hep-ph/9402256.

[42] J.M. Eisenberg, Y. Kluger, B. Svetitsky, «Pair Production in a Strong Electric Field with Back Reaction: An Interim Summary», *Acta Phys. Pol. B* **23**, 577 (1992).

[43] C. Banerjee, M.P. Singh, «Imprint of the temporal envelope of ultra-short laser pulses on the longitudinal momentum spectrum of e^+e^- pairs», *Phys. Rev. D* **105**, 076021 (2022), arXiv:1807.06951 [physics.plasm-ph].

[44] J.C.R. Bloch, C.D. Roberts, S.M. Schmidt, «Memory effects and thermodynamics in strong field plasmas», *Phys. Rev. D* **61**, 117502 (2000), arXiv:nucl-th/9910073.

[45] S.M. Schmidt *et al.*, «Non-Markovian effects in strong field pair creation», *Phys. Rev. D* **59**, 094005 (1999), arXiv:hep-ph/9810452.

[46] https://www.mathworks.com/help/matlab/ref/ode113.html

[47] A.V. Filatov, A.V. Prozorkevich, S.A. Smolyansky, V.D. Toneev, «Inertial mechanism: Dynamical mass as a source of particle creation», *Phys. Part. Nucl.* **39**, 886 (2008), arXiv:0710.0233 [hep-ph].

[48] H.H. Fan, C.W. Zhang, S. Tang, B.S. Xie, «Vortex state properties in multiphoton scalar pair production», *Phys. Rev. D* **111**, 076017 (2025), arXiv:2411.11067 [hep-ph].

[49] D. Sah, M.P. Singh, «Pair Production in Time-dependent Electric Field at Finite Times», arXiv:2309.12079 [hep-ph].

[50] https://in.mathworks.com/help/matlab/ref/trapz.html